Dendritic cell maturation and chemotaxis is regulated by TRPM2-mediated lysosomal Ca^{2+} release

Adriana Sumoza-Toledo,[*,†,‡,§] Ingo Lange,[*,†] Hanna Cortado,[‡,§] Harivadan Bhagat,[‡,§] Yasuo Mori,[‖] Andrea Fleig,[*,†] Reinhold Penner,[*,†,1] and Santiago Partida-Sánchez[‡,§,1]

*Laboratory of Cell and Molecular Signaling, Center for Biomedical Research, Queen's Medical Center, Honolulu, Hawaii, USA; [†]John A. Burns School of Medicine, University of Hawaii; Honolulu, Hawaii, USA; [‡]Center for Microbial Pathogenesis, The Research Institute at Nationwide Children's Hospital, Columbus, Ohio; USA; [§]The Ohio State University College of Medicine, Columbus, Ohio; USA; and [‖]Department of Synthetic Chemistry and Biological Chemistry, Graduate School of Engineering, Kyoto University, Katsura Campus, Kyoto, Japan

ABSTRACT **Chemokines induce calcium (Ca^{2+}) signaling and chemotaxis in dendritic cells (DCs), but the molecular players involved in shaping intracellular Ca^{2+} changes remain to be characterized. Using siRNA and knockout mice, we show that in addition to inositol 1,4,5-trisphosphate (IP_3)-mediated Ca^{2+} release and store-operated Ca^{2+} entry (SOCE), the transient receptor potential melastatin 2 (TRPM2) channel contributes to Ca^{2+}release but not Ca^{2+} influx in mouse DCs. Consistent with these findings, TRPM2 expression in DCs is restricted to endolysosomal vesicles, whereas in neutrophils, the channel localizes to the plasma membrane. TRPM2-deficient DCs show impaired maturation and severely compromised chemokine-activated directional migration as well as bacterial-induced DC trafficking to the draining lymph nodes. Defective DC chemotaxis is due to perturbed chemokine-receptor-initiated Ca^{2+} signaling mechanisms, which include suppression of TRPM2-mediated Ca^{2+} release and secondary modification of SOCE. DCs deficient in both TRPM2 and IP_3 receptor signaling lose their ability to perform chemotaxis entirely. These results highlight TRPM2 as a key player regulating DC chemotaxis through its function as Ca^{2+} release channel and confirm ADP-ribose as a novel second messenger for intracellular Ca^{2+} mobilization.—Sumoza-Toledo, A., Lange, I., Cortado, H., Bhagat, H., Mori, Y., Fleig, A., Penner, R., Partida-Sánchez, S. Dendritic cell maturation and chemotaxis is regulated by TRPM2-mediated lysosomal Ca^{2+} release. *FASEB J.* 25, 3529–3542 (2011). www.fasebj.org**

Key Words: ADP-ribose · calcium signaling · IP3R · SOCE

MIGRATION OF DENDRITIC CELLS (DCs) and other phagocytic cells to sites of infection and inflammation is a critical step toward an effective defense against pathogens (1–3). Phagocytes migrate throughout the body by following chemical cues from small molecules that are produced either endogenously (chemokines) or exogenously [microbially derived chemoattractants; *e.g.*, N-formylmethionyl-leucyl-phenylalanine (fMLP)]. DCs sense chemotactic signals *via* G-protein-coupled receptors (GPCRs) expressed on their plasma membrane (1, 4, 5). Although chemokine receptor stimulation elicits increases in intracellular Ca^{2+} ($[Ca^{2+}]_i$) in DCs (6–9), the ion channels that regulate the Ca^{2+} signals associated with chemokine-dependent migration of DCs remain unidentified.

The transient receptor potential melastatin-2 (TRPM2) is a calcium-permeable nonselective cation channel (10, 11) containing a Nudix-like region that binds and hydrolyzes ADP-ribose (ADPR) to ribose 5-phosphate and adenosine monophosphate (AMP) (10). ADPR binding to the Nudix-like domain induces cation currents across the plasma membrane, allowing Na^+ and Ca^{2+} influx (10, 11). TRPM2 gating by ADPR is facilitated further by the presence of nicotinic acid adenine dinucleotide phosphate (NAADP), cyclic ADPR (cADPR), hydrogen peroxide (H_2O_2), and Ca^{2+} (12–16), whereas channel activity is regulated negatively by AMP and permeating protons (pH; refs. 10, 17, 18). In addition to its role as a cation channel in the plasma membrane, TRPM2 functions as a lysosomal calcium-release channel in the rat pancreatic cell line INS-1 (19).

TRPM2 is expressed in the plasma membrane of human and mouse polymorphonuclear neutrophils (PMNs), monocytes (19–22), and Jurkat T cells (23). A recent study indicates that TRPM2 represents a key inflammatory mediator in cells of myeloid origin and that TRPM2-deficient mice are more resistant to induced experimental colitis due to defective chemokine production by monocytes and reduction of PMN infil-

[1] Correspondence: S.P.-S., Center for Microbial Pathogenesis, The Research Institute at Nationwide Children's Hospital, 700 Children's Dr., Columbus, OH 43205, USA. E-mail: santiago.partida-sanchez@nationwidechildrens.org; R.P., Center for Biomedical Research, The Queen's Medical Center, 1301 Punchbowl St., Honolulu, HI 96813, USA. E-mail: rpenner@hawaii.edu

doi: 10.1096/fj.10-178483

This article includes supplemental data. Please visit *http://www.fasebj.org* to obtain this information.

tration (21). In addition, earlier studies have shown defects in chemotaxis of phagocytes treated with the ADPR antagonist 8Br-ADPR due to a reduction of $[Ca^{2+}]_i$ on chemotactic stimuli (9), which suggests that ADPR regulates Ca^{2+} signaling following chemokine receptor stimulation. The relevance of ADPR/TRPM2 signaling pathway for DC biology has not been addressed.

In the present study, we investigated the role of TRPM2 channel during Ca^{2+} homeostasis and function of DCs. Our results show that TRPM2 function regulates $[Ca^{2+}]_i$ and is required for optimal DC maturation and chemotaxis. DCs express TRPM2 preferentially in endolysosomal compartments, which release Ca^{2+} on intracellular ADPR or external chemokine stimulation. Depletion of TRPM2 in DCs reduces chemokine-induced release of Ca^{2+} and secondarily reduces Ca^{2+} entry through store-operated pathways. Consequently, TRPM2-deficient DCs exhibit impaired chemotaxis in response to chemokines and the absence of both TRPM2 and inositol 1,4,5-trisphosphate receptor (IP_3R) abolishes chemotaxis altogether. Our data reveal a crucial role of TRPM2 in the regulation of Ca^{2+} signaling of DCs and provide additional support for the emerging concept of TRPM2 as a potential therapeutic target for inflammatory diseases.

MATERIALS AND METHODS

Animals

C57BL/6 wild-type (WT) mice and EGFP-C57BL/6 [C57BL/6-Tg (ACTB-EGFP) 131Osb/LeySopJ] mice were purchased from The Jackson Laboratory (Bar Harbor, ME, USA). Mice deficient in TRPM2, C57BL/6J.129 *trpm2*$^{-/-}$, were generated as described previously (21). EGFP-*trpm2*$^{-/-}$ mice were produced by crossing EGFP-C57BL/6 mice and C57BL/6J.129 *trpm2*$^{-/-}$ mice. All mice used in this study were bred and maintained under specific pathogen-free conditions at the animal facilities of The Research Institute at Nationwide Children's Hospital (Columbus, OH, USA) and the University of Hawaii (Honolulu, HI, USA). Mice were 8–12 wk old at the time of the experiments. All protocols involving rodents have been reviewed and approved by the institutional laboratory animal care and use committees at the Research Institute at Nationwide Children's Hospital and the University of Hawaii.

Reagents and antibodies

CXCL12, CCL19, and mGM-CSF were acquired from R&D Systems (Minneapolis, MN, USA). The anti-mouse CD11c biotin, CD11c allophycocyanin (APC), CD11b eFluor 605, Gr-1 biotin, CD16/32, CXCR4 phycoeritrin (PE), CCR7 PE, CCR5, CD80 PE, CD86 PE, MHC II PE, and CD83 purified rat anti-mouse I-A/I-E antibodies, were purchased from eBioscience (San Diego, CA, USA). Monoclonal mouse anti-Rab5 (clone Rab5–65), mouse anti-Rab7 (clone Rab7–117) antibodies, ADPR, AMP, bafilomycin A, and concanamycin A were from Sigma (St. Louis, MO, USA). EEAI antibody was from Santa Cruz Biotechnology (Santa Cruz, CA, USA). The rabbit anti-human TRPM2 was acquired from Bethyl Laboratories (Montgomery, TX, USA), and the rabbit anti-mouse TRPM2 was produced in our laboratory as described previously (24). Mouse monoclonal antibody (mAb) to lysosome-associated membrane protein 1 (LAMP1; Ly1c6), mouse mAb to 58K Golgi protein, and mouse antibody anti-PDI protein were purchased from Abcam (Boston, MA, USA). Alexa Fluor 488-goat anti-rabbit IgG, Alexa Fluor 568-goat anti-mouse IgG, Alexa Fluor 568-goat anti-rat IgG, and MitoTracker red were purchased from Invitrogen (Carlsbad, CA, USA). DC-LAMP antibody was from Beckman Coulter (Fullerton, CA, USA). 8-Br-ADPR was a generous gift from Tim Walseth (University of Minnesota, Minneapolis, MN, USA).

Phagocytic cell isolation

Mouse bone marrow (BM) was prepared from femurs and tibiae. PMNs were purified by positive selection using biotinylated anti-Gr-1 antibody and MACS streptavidin microbeads (Miltenyi Biotec, Auburn, CA, USA) following the manufacturer instructions. PMN purity was ≥95% as assessed by flow cytometry. BM-derived immature DCs (BMDCs) were generated *in vitro* by culture of 0.5×10^6 BM cells/ml in RPMI medium (ATCC, Manassas, VA, USA) supplemented with 7% FBS (v/v; Hyclone, South Logan, UT, USA), 50 μM 2-β-mrcaptoethanol (Sigma-Aldrich), 10 μg/ml penicillin/streptomycin, and 20 ng/ml mGM-CSF for 5–6 d. BMDCs were matured by stimulating the culture with TNF-α (10 ng/ml; Invitrogen) overnight at d 5. Cells were used for experiments 24 h later. Where indicated, $CD11c^+$ DCs were selected by magnetic sorting using biotinylated anti-CD11c antibody (eBioescence) and MACS streptavidin microbeads (Miltenyi Biotec). BMDC purity was ≥95% as assessed by flow cytometry. Splenic DCs were obtained by pretreatment of spleen tissues with collagenase D (1 mg/ml) before mechanical disaggregation.

Immunofluorescence

For TRPM2 staining, BMDCs and PMNs were attached to coverslips, pretreated with poly-L-lysine, for 20 min at room temperature. Cells were then fixed with 2% paraformaldehyde for 15 min at room temperature. Samples were permeabilized with 0.2% Triton X-100 for 5 min. Cells were then rinsed with PBS and blocked with 10% goat serum or 2% BSA for 30 min at 37°C. For TRPM2 detection, cells were incubated with rabbit preimmune serum as a negative control, or rabbit anti-mouse TRPM2 serum, or TRPM2 immune serum plus blocking peptide or polyclonal rabbit anti-human TRPM2 antibody, for 1 h at 37°C. Alexa Fluor 488 anti-rabbit IgG was used as secondary antibody. For detection of subcellular organelles, TRPM2-stained cells were further incubated with mouse anti-LAMP1, mouse anti-58K Golgi protein, mouse anti-PDI protein, mouse anti-human DC-LAMP, purified rat anti-mouse I-A/I-E, mouse anti-Rab5 or anti-Rab7, or the mitochondrion-selective dye MitoTracker red. Alexa Fluor 568 anti-mouse IgG was used as secondary antibody. Samples were mounted using Prolong Gold antifade reagent (Invitrogen). Samples were analyzed using the Zeiss 510 LSM Meta confocal laser scanning microscope and Zeiss LSM Image Browser program (Carl Zeiss, Hudson, OH, USA).

Flow cytometry

BMDCs were cultured in the presence of 20 ng/ml GM-CSF and then split into halves at d 5. Half of the culture was induced to mature by adding 10 ng/ml TNF-α (d 5); the other half was left untouched. On d 6, immature and mature BMDCs were stained with fluorescent anti-CD11c, CD11b, MHC class-II, CD80, CD83, CD86, CXCR4, CCR7, and CCR5

PE and analyzed using an LSR-II flow cytometer (BD Biosciences, San Jose, CA, USA). Splenic DCs were stained with fluorescent anti-CD11c, CD11b, MHC class-II, CD80, CD83, and CD86 PE and analyzed using an LSR-II flow cytometer.

TRPM2 mRNA detection

Total RNA was extracted from fresh isolated PMNs, immature DCs (5–6 d of culture and $CD11c^+$ selected) using TRIzol reagent (Invitrogen). cDNA was prepared by reverse transcription using SuperScript III RNase H-Reverse Transcriptase (RT) and oligo (dT). For TRPM2, PCR reactions were performed using the specific primer pair mTRPM2 3380 sense 5′-CAGATCCCAACCTACATTGACG-3′ and mTRPM2 3594 antisense 5′-GAAGGTGTAGTTGAACATGGCGA-3′. A 215-bp TRPM2-PCR product was detected after 30 cycles of amplification: 30 s at 94°C, annealing for 30 s at 46°C, and extension for 40 s at 72°C, followed by a final extension for 10 min. For GADPH, PCR reactions used the specific primer pair mGADPH 563 sense 5′-ACCACAGTCCATGCCATCAC-3′ and mGADPH 1014 antisense 5′-TCCACCACCCTGTTGCTGTA-3′. A 451-bp GADPH-PCR product was detected after 30 cycles of amplification: 30 s at 94°C, annealing for 30 s at 53°C, and extension for 40 s at 72°C, followed by a final extension for 10 min. For real-time PCR, total RNA extraction was performed using the Qiagen RNeasy Mini kit (Qiagen, Valencia, CA, USA). Complementary DNA from 1 μg of RNA was synthesized using a high-capacity cDNA synthesis kit (Applied Biosystems, Foster City, CA, USA). The cDNA was then subjected to quantitative real-time PCR reaction using a TaqMan qTR-PCR assay with predesigned probe and primers for mouse TRPM2 (Mm00663098_m1), GAPDH (Mm99999915_q1) and CD86 (Mm00444543_m1) (Applied Biosystems).

Chemotaxis assay

Chemotaxis assays were performed using 24- or 96-transwell plates (Costar, Corning, NY, USA) with 5-μm-pore polycarbonate filter. For standard chemotaxis assay (25). chemoattractants were diluted in HBSS and placed in the lower chamber, whereas 5×10^5 immature or mature DCs were added to the upper chamber of the transwell. The checkerboard chemotaxis assay was performed by placing chemoattractants on the bottom chamber only (chemotaxis), or on the top chamber only (chemokinesis), or both (chemokinesis) as described previously (26). After incubation of the chambers for 90 min at 37°C, the transmigrated cells were collected from the lower chamber, fixed, and counted by flow cytometry. The results are expressed as the mean ± SE of the chemotaxis index (CI) for triplicate wells. The CI represents the fold-change in the number of migrated cells in response to the chemoattractant divided by the basal migration of cells migrating in response to control medium. Similar experiments were performed using DCs transfected with scrambled siRNA and specific TRPM2-siRNA.

Dendritic cell migration *in vivo*

Immature BMDCs (2×10^6/50 μl) cultured for 5 d from EGFP-*trpm2*$^{-/-}$ mice or control mice (EGFP-C57BL/6) were injected in the right footpad of C57BL/6 mice 2 h before injection of *Escherichia coli* (1×10^6 bacteria/footpad). Single-cell suspensions from the right side popliteal and inguinal draining lymph nodes and nondraining lymph nodes (left side controls) were incubated with fluorescent anti-CD11c, and anti-MHC class-II, CD11b and analyzed by flow cytometry.

TRPM2 depletion by siRNA

Specific siRNA sequences for TRPM2 (Entrez Gene ID 28240) were selected from the murine HP GenomeWide siRNA oligos available from Qiagen; 3′ Cy5-labeled siRNA oligos were synthesized and annealed by the manufacturer. Scrambled siRNA sequences were used as negative controls. siRNA transfection was carried out using the GeneSilencer siRNA transfection reagent (Gene Therapy Systems, San Diego, CA, USA). BMDCs (d 5) were washed and plated in 6-well plates at 2.5×10^6 in 1 ml of serum-free RPMI 1640. Annealed siRNA ($\leq$ 20 mM) was incubated with GeneSilencer reagent following the manufacturer's protocol. Transfection mixture was then added to the DC culture. Mock controls were transfected with GeneSilencer siRNA transfection reagent alone.

Electrophysiology

For patch-clamp experiments, cells were kept in standard Ringer's solution: 140 mM NaCl, 2.8 mM KCl, 1 mM $CaCl_2$, 2 mM $MgCl_2$, 10 mM glucose, and 10 mM HEPES (pH 7.2 adjusted with NaOH). Standard pipette-filling solutions contained 140 mM Cs-glutamate, 8 mM NaCl, 1 mM $MgCl_2$, and 10 mM HEPES (pH 7.2 adjusted with CsOH). Experiments were performed under Ca^{2+}-buffered or unbuffered conditions (as indicated). ADPR was added to its final concentrations as appropriate. DCs were rinsed once with extracellular solution and transferred to coverslips. Patch-clamp experiments were performed in the whole-cell configuration at 21–25°C. All data were acquired with Pulse software controlling an EPC-9 amplifier (Heka, Lambrecht, Germany) and analyzed using FitMaster (Heka) and Igor Pro (WaveMetrics, Lake Oswego, OR, USA). Voltage ramps of 50 ms spanning the voltage range from −100 to +100 mV were delivered from a holding potential of 0 mV at a rate of 0.5 Hz over a period of 200–500 s. Voltages were corrected for liquid junction potentials. Currents were filtered at 2.9 kHz and digitized at 100-μs intervals. Capacitive currents and series resistance were determined and corrected before each voltage ramp. The ramp current amplitudes at −80 mV (inward current) were extracted from individual ramp data and displayed as current development over time. Some individual ramps were displayed as representative current-voltage (*I-V*) relationships.

Ca^{2+} measurements

For Ca^{2+} measurements, cells were loaded with 5 μM Fura-2-AM (acetoxymethylester; Molecular Probes, Eugene, OR, USA) for 30 min in medium at 37°C. Balanced Ca^{2+} experiments were then performed with subsequent patch-clamp experiments where 200 μM Fura-2 (pentapotassium salt; Molecular Probes) was added to the standard internal solution to ensure continuous Fura-2 signals. The cytosolic Ca^{2+} concentration of individual patch-clamped cells was monitored at a rate of 5 Hz with a dual excitation fluorometric system using a Zeiss Axiovert 200 fluorescence microscope equipped with a ×40 LD AchroPlan objective. The monochromatic light source (monochromator B; TILL Photonics, Lambrecht, Germany) was tuned to excite Fura-2 fluorescence at 360 and 390 nm for 20 ms each. Emission was detected at 450–550 nm with a photomultiplier, whose analog signals were sampled and processed by X-Chart software (Heka). Fluorescence ratios (F_{360}/F_{390}) were translated into free intracellular Ca^{2+} concentration based on calibration parameters derived from patch-clamp experiments with cali-

brated Ca^{2+} concentrations. For IP_3 experiments, cells were permeabilized with 4 μM digitonin and exposed to 100 μM IP_3.

For Ca^{2+} measurements in intact cells, Fura-2-AM preloaded-CD11c$^+$ DCs were stimulated with 300 ng/ml CXCL12 (immature DCs) or 75 ng/ml CCL19 (mature DCs) in the presence or absence of 1 mM $CaCl_2$ at 30 s. To obtain Ca^{2+}-free conditions, external Ca^{2+} was washed out with zero Ca^{2+} external Na^+-Ringer for 60 s prior to the stimulation with the specific chemoatractant. Ca^{2+} responses were monitored using a CCD camera-based Ca^{2+} imaging system (TILL Photonics). Ca^{2+} signal patterns were defined as follows: a Ca^{2+} spike or Ca^{2+} transient was defined as a rapidly rising transient increase in $[Ca^{2+}]_i$ of ≥10 nM above baseline $[Ca^{2+}]_i$ in resting conditions; multiple $[Ca^{2+}]_i$ transients arising periodically from a stable baseline were considered Ca^{2+} oscillations; and the slower rising wave-like phase of sustained Ca^{2+} entry was considered a Ca^{2+} plateau phase. Experiments were analyzed using Igor Pro software; areas under individual Ca^{2+} transients (integral in μM*s), and the initiation times (s) of the Ca^{2+} plateau phase were calculated using the multipeak fit analysis function in Igor Pro. Intracellular Ca^{2+} concentration $[Ca^{2+}]_i$ was determined following the formula $f(x) = K_D\ [(R - R_{min})/(R_{max} - R)]$, where K_D is the K_D for BAPTA, R_{min} is the ratiometric measurement of the internal Ca^{2+} clamped to 0 (10 mM BAPTA), R_{max} is the ratiometric measurement of internal Ca^{2+} clamped at saturating Ca^{2+} (1 mM), and r is the ratiometric measurement of intracellular Ca^{2+} on chemokine stimulation.

Ca^{2+} measurement by flow cytometry

For Fluo-3 flow cytometry assays, immature BMDCs were resuspended in cell-loading medium (HBSS with 1 mM Ca^{2+}, 1 mM Mg^{2+}, 1% FBS, and 4 mM probenecid) at 5×10^6 cells/ml and loaded with the calcium-sensitive dye Fluo-3 AM (4 μg/ml; Invitrogen). Cells were stimulated with CXCL12 chemokine, and the accumulation of intracellular free Ca^{2+} was assessed by FACS over the next 200 s by measuring the fluorescence emission of Fluo-3 in the FL-1 channel. Data were analyzed with FlowJo software (Tree Star, Inc., Ashland, OR, USA) using the kinetic platform.

Statistical analysis

Data are expressed as mean ± SE values. Statistical evaluation was determined by unpaired Student's t test or 1-way ANOVA test where appropriate by using GraphPad Prism software (GraphPad, San Diego, CA, USA). The algorithms Kolmogorov-Smirnov (K-S) and probability binning [$\chi(T)$ or PB] and FlowJo software were used for statistical comparison of FACS data. A value of $P < 0.05$ was considered to be statistically significant.

RESULTS

Differential cellular compartmentalization of TRPM2 in phagocytes

To assess the functionality of TRPM2 channels in dendritic cells, we first examined the expression of TRPM2 transcripts in various tissues and cell types, including PMNs, spleen T cells, and bone marrow-derived DCs (BMDCs) from C57BL/6 mice. **Figure 1*A*** shows that TRPM2 mRNA was highly expressed in PMNs and BMDCs when compared to the DC cell line DC 2.4. TRPM2 transcripts were nearly undetectable in T cells and 3T3 fibroblasts (Fig. 1*A*). Consistent with previous reports (27, 28), TRPM2 was greatly expressed in the brain (Fig. 1*A*). Since TRPM2 expression and activation is well documented in human PMNs (20, 22, 29), we next examined the cellular distribution of TRPM2 in PMNs and BMDCs by immunofluorescence. We stained PMNs and BMDCs with an anti-human TRPM2 antibody (Fig. 1*B*) or an anti-mouse TRPM2 antibody (Supplemental Fig. S1), while the nucleus was visualized with either DAPI (Fig. 1*B*) or propidium iodine (Supplemental Fig. S1). As evident in Fig. 1*B*, we observed plasma membrane expression of TRPM2 in mouse PMNs, similar to what has been reported for human PMNs (22, 29). Interestingly, TRPM2 exhibited a punctate cytoplasmic distribution in immature BMDCs (Fig. 1*B*). Moreover, we did not detect any TRPM2 signal in 3T3 cells or when a specific blocking peptide was used together with the anti-human TRPM2 antibody (data not shown) or when we used mouse preimmune serum (Supplemental Fig. S1). A similar subcellular pattern of TRPM2 expression was observed using either anti-human or anti-mouse TRPM2 antibodies.

ADPR does not induce TRPM2 plasma membrane currents in DCs

To confirm whether TRPM2 was present in the plasma membrane of PMN but not BMDCs, we assessed TRPM2 channel expression directly using whole-cell patch-clamp recordings. Intracellular perfusion of mouse PMN with 10 μM ADPR elicited a large current that rapidly developed after establishment of the whole cell configuration (Fig. 1*D*, black circles). The currents induced by ADPR had identical *I-V* relationships (Fig. 1*E*) to those of heterologously expressed TRPM2 channels (10). Figure 1*C* illustrates the ADPR-TRPM2 dose-response in mouse PMNs, with an EC_{50} of ~540 nM, slightly more sensitive than in PMNs isolated from human blood (EC_{50} ~1 μM; refs. 22, 29). To distinguish TRPM2 currents from leak currents, we replaced extracellular Na^+ with *N*-methyl-D-glucamine ($NMDG^+$; an impermeable cation), resulting in complete suppression of inward current (Fig. 1*D*). Figure 1*E* (gray trace) shows the TRPM2 *I-V* relationship under $NMDG^+$ conditions. In contrast to PMNs, ADPR at concentrations of up to 1 mM failed to induce any currents in immature BMDCs (Fig. 1*D*, blue circles) and mature BMDCs (Supplemental Fig. S2*A*), demonstrating the absence of functional TRPM2 channels in the plasma membrane of BMDCs. Furthermore, the quantitative analysis of TRPM2 mRNA expression in TNF-α stimulated-BMDCs shows that TRPM2 is not up- or down-regulated on TNF-α treatment, whereas up-regulation of the costimulatory molecule CD86 indicates that maturation of BMDCs occurred (Supplemental Fig. S2*B*).

ADPR causes Ca^{2+} release in mouse DCs by gating TRPM2 channels

Because of the predominant intracellular expression of TRPM2 in BMDCs, we reasoned that it might function

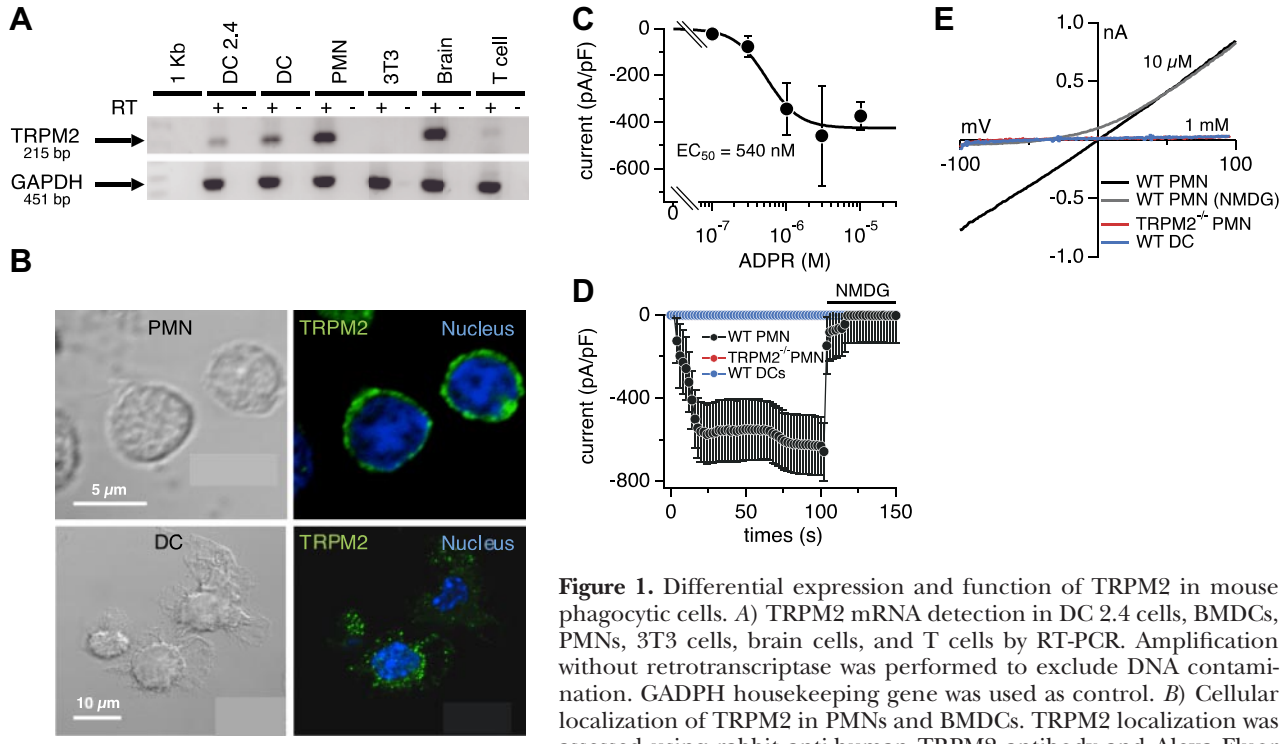

Figure 1. Differential expression and function of TRPM2 in mouse phagocytic cells. *A*) TRPM2 mRNA detection in DC 2.4 cells, BMDCs, PMNs, 3T3 cells, brain cells, and T cells by RT-PCR. Amplification without retrotranscriptase was performed to exclude DNA contamination. GADPH housekeeping gene was used as control. *B*) Cellular localization of TRPM2 in PMNs and BMDCs. TRPM2 localization was assessed using rabbit anti-human TRPM2 antibody and Alexa Fluor 488-anti-rabbit IgG as secondary antibody. Images are representative of >3 independent experiments. *C*) Dose-response curve of TRPM2 currents in response to increasing concentrations of intracellular ADPR in mouse PMNs. Cells were kept in standard external solution supplemented with 1 mM Ca^{2+}. Cells were perfused with standard Cs-glutamate-based internal solution supplemented with ADPR as indicated and in the absence of Ca^{2+} buffers (unbuffered conditions). Data were acquired using a 50-ms voltage ramp from −100 to +100 mV given at 0.5 Hz. Current amplitudes were extracted at −80 mV, normalized to cell size (in pF), averaged, and plotted *vs.* the respective ADPR concentration (n=5–6 for each data point). The half-maximal excitatory concentration (EC_{50} 540 nM) and Hill coefficient (Hill 2) was estimated using a dose-response fit. Error bars = SEM. *D*) Average TRPM2 currents in WT PMNs with 10 μM ADPR added to the internal solution (n=11; black circles). $NMDG^+$ was applied to distinguish TRPM2 currents from leak (black bar). In PMNs isolated from $TRPM2^{-/-}$ mice, no currents developed with 1 mM ADPR (n=10; red circles). WT BMDCs did not develop any TRPM2 currents in response to perfusion with 1 mM ADPR in the internal solution (n=6; blue circles). *E*) Representative *I-V* relationships of ADPR-induced currents in WT PMNs (black trace; extracted at 44 s), WT PMNs plus $NMDG^+$ (black trace; extracted at 110 s), $TRPM2^{-/-}$ PMNs (red trace; extracted at 50 s) and WT BMDCs (blue trace; extracted at 100 s).

as a Ca^{2+} release channel. To test this hypothesis, we performed balanced Fura-2 experiments, measuring changes in intracellular Ca^{2+} in immature BMDCs preloaded with Fura-2-AM. Cells were then perfused intracellularly with 0.1–1000 μM ADPR in the presence of 200 μM Fura-2. Na^+-based solution without Ca^{2+} was applied externally before whole-cell break-in to avoid contribution of Ca^{2+} influx to the measured Ca^{2+} signals. **Figure 2*A*** shows that 1 μM of ADPR was sufficient to elicit significant $[Ca^{2+}]_i$ increases in BMDCs (blue line). The Ca^{2+} elevation was abrogated when BMDCs were perfused with ADPR along with 8-Br-ADPR (Fig. 2*B*, black line) or 100 μM AMP (Fig. 2*B*, blue line), which are both known TRPM2 channel inhibitors. Similar results were obtained in mature BMDCs perfused with 10 μM ADPR (n=5, Fig. S2C). These responses were mediated by TRPM2, since even 1 mM ADPR failed to induce Ca^{2+} release in BMDCs generated from $TRPM2^{-/-}$ mice (Fig. 2*B*, red line). We also investigated whether TRPM2 might function as a Ca^{2+} release channel in PMN isolated from BM of WT mice. PMNs were loaded with Fura-2-AM and subsequently perfused with standard internal solution supplemented with 100 μM ADPR and 200 μM Fura-2. Figure 2*C* shows that ADPR did not elicit measurable intracellular Ca^{2+} increase in mouse PMNs. These results identify TRPM2 exclusively as a Ca^{2+} release channel in DCs but not in PMNs.

DCs express TRPM2 in late endosomal and lysosomal compartments

To determine the TRPM2 localization within BMDCs, we performed costaining of TRPM2 and subcellular organelles. Confocal microscopy analysis revealed well-defined intracellular structures containing TRPM2 (**Fig. 3**). TRPM2 did not significantly colocalize with structures expressing the endoplasmic reticulum (ER) marker protein disulfide isomerase (PDI; Fig. 3*A*, top panels[b]) or the Golgi apparatus expressing the 58K Golgi protein (Fig. 3*A*, middle panels), or with the mitochondrial marker MitoTracker (Fig. 3*A*, bottom panels[b]). Instead, TRPM2 showed a punctate cyto-

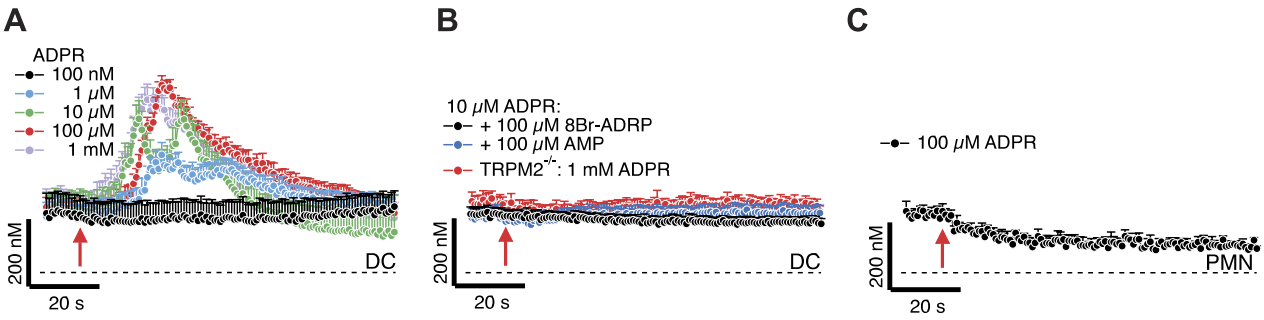

Figure 2. TRPM2 functions as Ca^{2+} release channel in mouse DCs but not PMNs. BMDCs and PMNs isolated from WT and TRPM2$^{-/-}$ mice were loaded with 5 μM Fura-2-AM. Calcium mobilization was analyzed using the whole-cell patch-clamp configuration where the standard internal solution was supplemented with various concentrations of agonist/antagonist and 200 μM Fura-2. Red arrow indicates whole-cell break-in. Just before break-in, the standard extracellular solution was switched from 1 mM Ca^{2+} to 0 Ca^{2+} to isolate release events. *A*) Average Ca^{2+} release in BMDCs induced by perfusion of cells with increasing concentrations of ADPR (n=6–8). *B*) Average inhibition of ADPR-induced (10 μM) Ca^{2+} release in WT BMDCs by 100 μM 8-Br-ADPR (black trace, n=10) and 100 μM AMP (blue trace, n=11). Absence of ADPR-induced (1 mM) Ca^{2+} release in BMDCs isolated from TRPM2$^{-/-}$ mice (red trace, n=7). *C*) Absence of ADPR-induced (100 μM) Ca^{2+} release in PMNs isolated from WT mice (C57BL/6; n=4).

plasmic distribution that partially colocalized with LAMP1 in immature BMDCs (Fig. 3*B*). Although LAMP1 is widely accepted as lysosome marker, it may be also found in Golgi (30). To confirm the expression of TRPM2 channel in lysosomes, we detected another member of the LAMP family, DC-LAMP or LAMP3, which is expressed only in the endosomal or lysosomal compartment and is restricted to mature DCs (ref. 31 and Fig. 3*D*). We observed colocalization of TRPM2 and DC-LAMP in mature DCs, suggesting predominant expression of TRPM2 channels in lysosomal membranes of DCs.

Although TRPM2 was clearly associated with lysosomal organelles in both immature and mature BMDCs, the channel was not detected within the endocytic pathway, as we did not observe any colocalization of TRPM2 with early endosomes or late endosomes using antibodies against Rab5 or the transferrin receptor EEA1 and Rab7, respectively (Supplemental Fig. S2*D*). Furthermore, TRPM2 was not found in MHC-II-containing compartments (Supplemental Fig. S2*D*). To assess the lysosomal localization of TRPM2 functionally, immature BMDCs were treated for 30 min with 100 nM bafilomycin A1, a specific inhibitor of the vacuolar-type H^+-ATPase that empties lysosomal Ca^{2+} stores (32). This treatment completely suppressed the Ca^{2+} release in BMDCs perfused with 10 μM ADPR (Fig. 3*C*).

TRPM2-deficient DCs exhibit defective chemokine-induced Ca^{2+} signaling

Chemokines produce increases of $[Ca^{2+}]_i$ in DCs (9, 33); however, the calcium channels that control Ca^{2+} signals associated with the activation of chemokine receptors are not well known in these cells. To determine whether TRPM2-mediated Ca^{2+} release is activated during chemokine receptor signaling, we examined Ca^{2+} responses following chemokine stimulation (CXCL12 and CCL19; CXCR4 and CCR7 ligands in immature and mature DCs, respectively) in intact CD11c$^+$ immature and mature WT and TRPM2$^{-/-}$ BMDCs. We examined $[Ca^{2+}]_i$ patterns defined as Ca^{2+} spikes (single Ca^{2+} transients), Ca^{2+} oscillations (multiple Ca^{2+} transients) and plateau phases (sustained, wave-like Ca^{2+} increases) as described in Materials and Methods. The integral of Ca^{2+} spikes and beginning of the plateau phases were determined using the multipeak fit analysis function in Igor Pro software.

In the presence of 1 mM extracellular Ca^{2+} (**Fig. 4*A*–*E***), 54% of WT BMDCs (30/56 cells) responded with an average of 2.5 ± 0.4 Ca^{2+} oscillations within the first 300 s after stimulation with CXCL12 (n=56). This condition was followed by a secondary Ca^{2+} plateau phase at 327 ± 27 s after stimulation (Fig. 4*B*, black circles). Of the cells, only 46% (26/56 cells) developed the Ca^{2+} plateau phase at 311 ± 31 s without initial oscillations. Examples of these two types of Ca^{2+} responses of WT BMDC stimulated with CXCL12 are shown in Fig. 4*A*. In contrast, the majority of TRPM2$^{-/-}$ BMDCs (81% or 63/78 cells) showed no initial oscillations, and the remainder of cells had strongly reduced numbers of Ca^{2+} oscillations (1.5±0.2 oscillations; Fig. 4*A*, red trace; Fig. 4*B* inset, red circles; P<0.05). This condition was also evident from analysis of the Ca^{2+} integral of Ca^{2+} oscillations (Fig. 4*C*; P<0.05) as well as during the rising phase of the Ca^{2+} plateau (P<0.05). The Ca^{2+} plateau phase began at a similar time point as in WT BMDCs (313±35 s in cells with oscillation, n=15; and 300±15 s in cells with no initial oscillation, n=63) but reached slightly lower levels of $[Ca^{2+}]_i$ (P<0.05; Fig. 4*B*).

Mature WT BMDCs rarely showed oscillations of intracellular Ca^{2+} in response to CCL19 (Fig. 4*D*, *E*), and the Ca^{2+} plateau phase developed with a delay of 651 ± 23 s (n=30) after stimulation (Fig. 4*E*, black circles; *F*, black bar). Mature TRPM2$^{-/-}$ BMDCs responded slightly earlier (Fig. 4*F*, red bar) to chemokine stimulation (486±39 s; n=11; P<0.01); however, the Ca^{2+} signal tapered off faster than in WT and to a lower overall level within the measured time frame (Fig. 4*E*, red circles). Thus, although TRPM2 itself does not directly contribute to Ca^{2+} entry as a plasma membrane

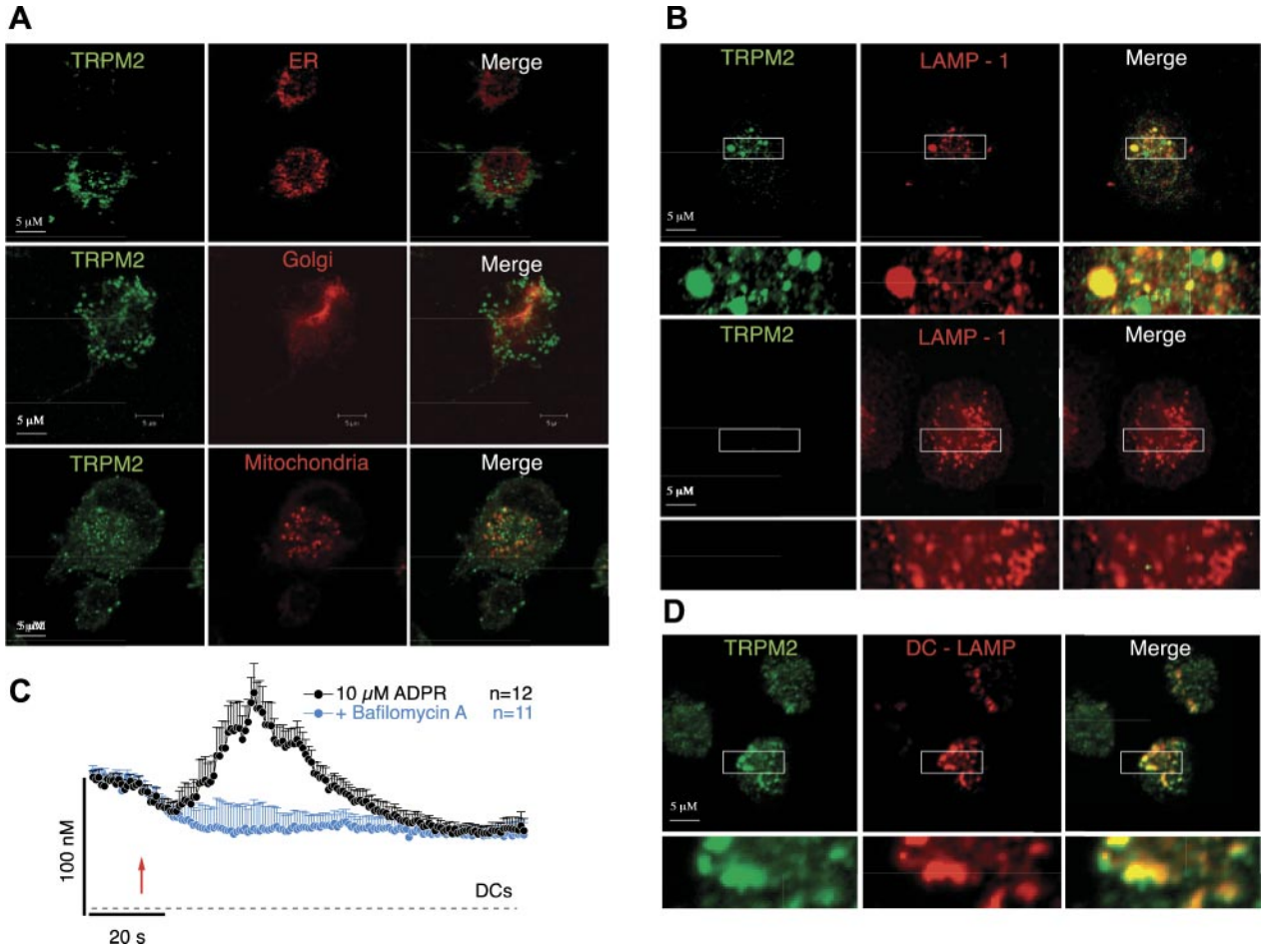

Figure 3. Subcellular localization of TRPM2 is restricted to endolysosomes in DCs. BMDCs were fixed with 2% PFA and permeabilized with 0.2% Triton-X100. TRPM2 localization was assessed using the rabbit anti-human TRPM2 polyclonal antibody, and Alexa Fluor 488-anti-rabbit IgG was used as secondary antibody. *A*) TRPM2 is not expressed in Golgi, ER, and mitochondria. Cells were costained with 58K Golgi protein (top panel), anti-mouse PDI protein antibody (middle panel) or Mitotracker Red (bottom panel). *B*) Top panels: immature BMDCs were costained with mouse anti-LAMP1 antibody. Bottom panels: TRPM2$^{-/-}$ BMDCs. *C*) Immature WT BMDCs were loaded with 5 μM Fura-2-AM for 30 min at 37°C. Average ADPR-induced (10 μM) Ca^{2+} release in WT BMDCs (black trace, n=12), and cells pretreated with 100 nM bafilomycin A1 for 30 min at 37°C (blue trace, n=11). 100 nM bafilomycin A1 was also added to the extracellular solution. Ca^{2+} mobilization was analyzed using patch-clamp. Red arrow indicates whole-cell break-in. Just before break-in, the extracellular solution was switched from 1 mM Ca^{2+} to 0 Ca^{2+} to isolate release events. *D*) TNF-α-matured BMDCs were costained with mouse anti-DC-LAMP. Confocal images are representative of >3 independent experiments. Insets: magnified view of boxed area in corresponding panel.

channel, its absence does appear to affect Ca^{2+} influx through chemokine signaling in DCs.

TRPM2 deficiency differentially affects Ca^{2+} release depending on DC maturity

Since TRPM2 acts as a Ca^{2+} release channel in DCs (Fig. 2), we examined Ca^{2+} signaling in the absence of external Ca^{2+} (**Fig. 5**). Two patterns of Ca^{2+} signals were observed in Ca^{2+}-free extracellular solution: cells responded with either a Ca^{2+} spike or with Ca^{2+} oscillations. These patterns were seen in both immature BMDCs stimulated with CXCL12 and mature BMDCs stimulated with CCL19. The relative amount of cells responding with a Ca^{2+} spike (~25% of immature cells and ~10% of mature BMDCs) or Ca^{2+} oscillations was comparable in WT and TRPM2$^{-/-}$ cells. As expected, the secondary phase never developed in the absence of extracellular Ca^{2+}, indicating that it was mainly carried by Ca^{2+} influx. No difference was observed in the delay of Ca^{2+} oscillations evoked by CXCL12 in WT and TRPM2$^{-/-}$ BMDCs (~200 s; Supplemental Fig. S3A). However, immature TRPM2$^{-/-}$ BMDCs that responded with a Ca^{2+} spike to a CXCL12 challenge had significantly smaller Ca^{2+} spikes compared to WT (Fig. 5*A*), as assessed by the integral of individual Ca^{2+} spikes (Fig. 5*B*, $P<0.05$). The inset in Fig. 5*A* represents a typical release transient measured in a WT cell over the course of 300 s of experimental time.

In contrast to immature cells, the amplitudes and delays of Ca^{2+} spikes in mature BMDCs stimulated with CCL19 were identical in WT and TPRM2$^{-/-}$ BMDCs (Fig. S3C). Mature cells with Ca^{2+} oscillations also had indistinguishable initial responses to the chemokine

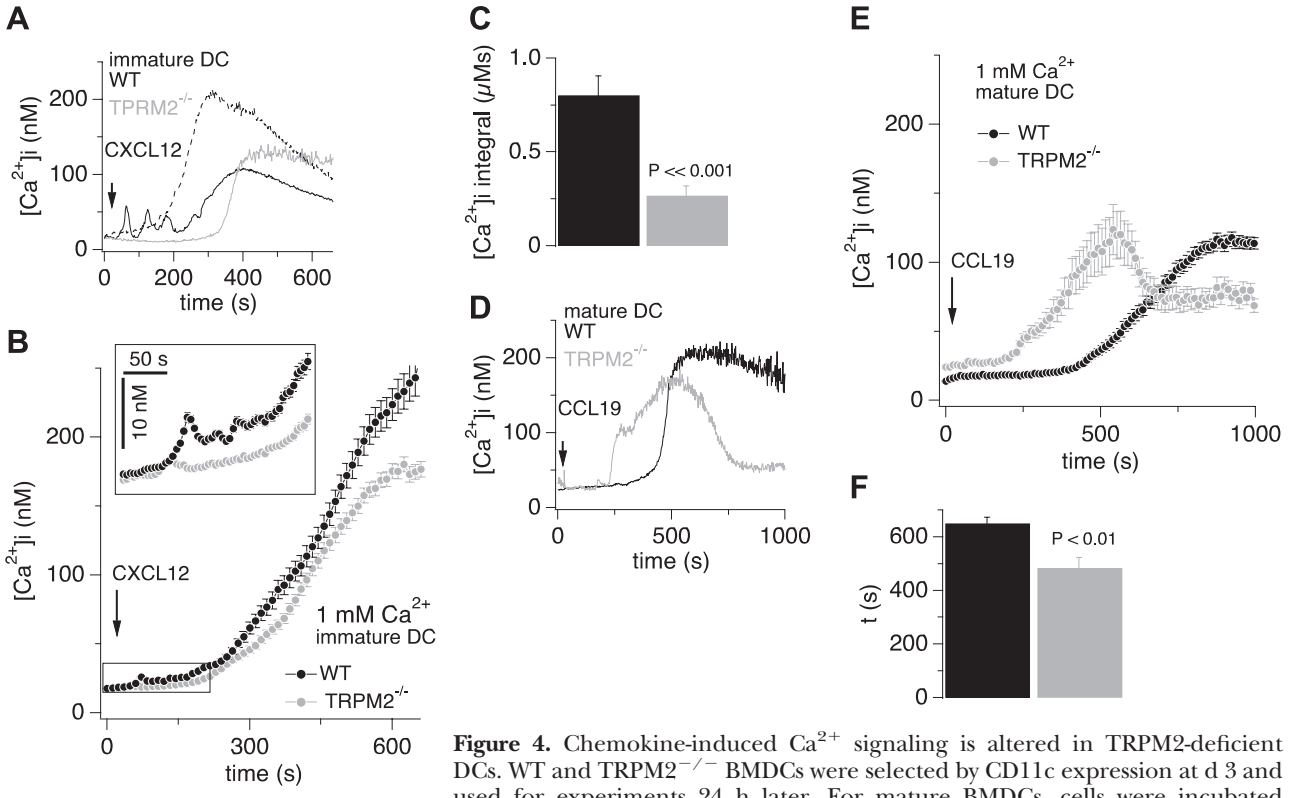

Figure 4. Chemokine-induced Ca^{2+} signaling is altered in TRPM2-deficient DCs. WT and TRPM2$^{-/-}$ BMDCs were selected by CD11c expression at d 3 and used for experiments 24 h later. For mature BMDCs, cells were incubated overnight with 10 ng/ml TNF-α. BMDCs were loaded with 5 μM Fura-2-AM. Error bars = SEM. *A*) Representative Ca^{2+} responses of an immature WT (black trace and dashed trace) and a TRPM2$^{-/-}$ (red trace) BMDC to 300 ng/ml CXCL12 in the presence of 1 mM external Ca^{2+} (arrow indicates application). *B*) Average CXCL12-induced Ca^{2+} response of immature WT (black circles, n=56) or TRPM2$^{-/-}$ (red circles, n=78) BMDCs. Box magnifies the oscillatory phase during the first 216 s. *C*) Integral of individual Ca^{2+} oscillations (see Materials and Methods) assessed during the first 300 s of experimental time in both WT (black bar, n=74 spikes) and TRPM2$^{-/-}$ BMDCs (red bar, n=28 spikes). *D*) Representative Ca^{2+} responses of a mature WT (black trace) and a TRPM2$^{-/-}$ (red trace) BMDC to 75 ng/ml CCL19 in the presence of 1 mM external Ca^{2+} (arrow indicates application). *E*) Average CCL19-induced Ca^{2+} responses in mature WT (black circles, n=35) or TRPM2$^{-/-}$ (red circles, n=11) BMDCs. *F*) Average initiation time of the Ca^{2+} plateau phase in WT (black bar, n=30) and TRPM2$^{-/-}$ BMDCs (red bar, n=11). Traces were lined up to the cell with lowest basal calcium.

(Fig. 5*C*, first Ca^{2+} transient), and the Ca^{2+} oscillations observed in WT (9.5±0.6 transients) and TRPM2$^{-/-}$ BMDCs (8.3±0.6 transients) did not differ. However, except for the first transient, Ca^{2+} oscillations measured in TRMP2$^{-/-}$ cells were strongly reduced in amplitude, resulting in an overall suppressed Ca^{2+} signal compared to WT (Fig. 5*C*). This was also evident in the integral of all Ca^{2+} oscillations between 0 and 500 s (including the first transient) in individual WT and TRPM2-deficient cells (Fig. 5*D*; P<0.05). The inset in Fig. 5*C* presents a typical release transient measured in a WT cell. Similar to experiments performed with CCL19 in the presence of extracellular Ca^{2+} (Fig. 4*E*), mature BMDCs responding to chemokine stimulation with Ca^{2+} oscillations developed Ca^{2+} transients earlier in TRPM2$^{-/-}$ BMDCs than in WT BMDCs (223±16 s in WT *vs.* 174±15 s in TRPM2$^{-/-}$ cells; P<0.02).

TRPM2-mediated Ca^{2+} signaling is required for optimal DC maturation

Since the regulation of Ca^{2+} is essential for DC maturation and function (33, 34) and because we found that TRPM2 deficiency affects Ca^{2+} release in DCs, we next examined whether TRPM2-dependent Ca^{2+} signals are required during DC differentiation, maturation and migration *in vitro* as well as *in vivo*. BMDCs were prepared from WT and TRPM2$^{-/-}$ mice and the expression of DC lineage (CD11c^{+}) and maturation markers (MHC-II, CD80, CD86, and CD83) were analyzed by flow cytometry. Both BMDC cultures showed no significant difference in the proportion of CD11c^{+} cells at d 6 (**Fig. 6*A***), and cell proliferation rates were also similar (Fig. 6*B*). However, when TNF-α or CpG DNA (TLR9 activator) were used as maturation stimulus, a smaller fraction of CD11c^{+} TRPM2$^{-/-}$ BMDCs up-regulated Class-II, CD86, CD80, and CD83 molecules (Fig. 6*C*, red line) compared to TRPM2$^{+/+}$ BMDCs (Fig. 6*C*, black line). Furthermore, we quantitatively evaluated differences in the expression of each activation marker by applying the χ(T) or PB algorithm to determine whether two histograms are statistically significantly different (ref. 35 and Supplemental Table S1). The analysis revealed that stimulated TRPM2$^{-/-}$ BMDCs not only failed to reach optimal levels of maturation molecules but also showed that a greater

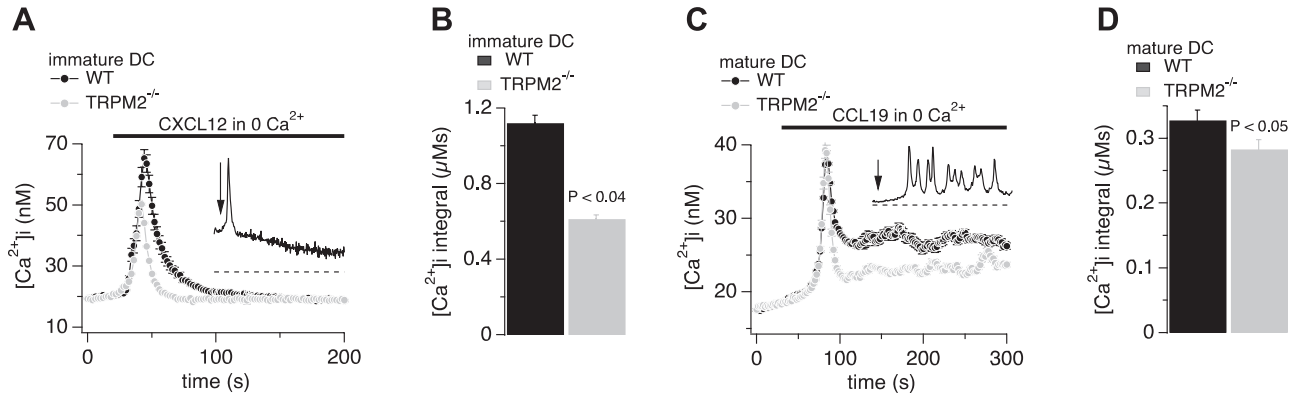

Figure 5. TRPM2 deficiency differentially affects Ca^{2+} release depending on DC maturity. BMDCs were isolated and treated as described in Fig. 4. Cells were maintained in standard external solution containing 1 mM Ca^{2+}. Extracellular Ca^{2+} was removed 1 min before the addition of chemokines (300 ng/ml of CXCL12 or 75 ng/ml of CCL19). Error bars = SEM. Peak of the first Ca^{2+} transient measured in each cell was aligned to the earliest peak recorded in each group (immature and mature BMDCs). No difference was found in response time to chemokine between WT and TRPM2$^{-/-}$ immature BMDCs ~ 200 s. Ca^{2+} spikes appeared earlier in TRPM2$^{-/-}$ (~170 s) than in WT (~200 s) mature BMDCs. *A*) Average Ca^{2+} release of immature WT (black circles; n=51) and TRPM2$^{-/-}$ BMDCs (red circles; n=81) responding with a Ca^{2+} spike on CXCL12 stimulation (black bar). Inset: data trace from an example WT cell. Arrow indicates chemokine application. *B*) Averaged Ca^{2+} integral of the Ca^{2+} spike in WT BMDCs (black bar, n=51) and TRPM2$^{-/-}$ BMDCs (red bar, n=81) taken from the data in *A*. *C*) Average Ca^{2+} responses of mature WT (black circles; n=96) and TRPM2$^{-/-}$ (red circles; n=96) BMDCs with Ca^{2+} oscillations induced by CCL19 stimulation (black bar). Inset: representative Ca^{2+} oscillation pattern measured in a WT cell. *D*) Averaged Ca^{2+} integral of Ca^{2+} oscillations measured in individual WT BMDCs (black bar, n=916 spikes) and TRPM2$^{-/-}$ BMDCs (red bar, n=798 spikes) taken from the data in *C*. A Ca^{2+} transient was defined as a peak if it showed an increase and decrease in Ca^{2+} of ≥10 nM following a normal Gaussian distribution. Graphs represent means of 3 independent experiments. Traces were lined up to the cell with lowest basal calcium.

proportion of these cells did not up-regulate maturation markers at all, as compared with their WT BMDC counterparts (Fig. 6*C*; histogram plot of difference, green line). These results indicate that a subpopulation of TRPM2$^{-/-}$ BMDCs cannot transition from an immature to a mature phenotype *in vitro*, even with a potent stimulus such as CpG-oligonucleotides (ODNs), which mimic bacterial CpG-DNA (36).

To determine the maturation status of DCs *in vivo*, we assessed lineage and maturation markers of DCs isolated from the spleen of WT and TRPM2$^{-/-}$ mice. We found a significant increase in the number of CD11b^{+}CD11c^{hi} DCs in TRPM2$^{-/-}$ mice (Fig. 6*D*); however, this population expressed lower levels of CD80 when compared to WT CD11b^{+} CD11c^{hi} DCs (Fig. 6*E*). Although the number of CD11b^{+}CD11c^{int} DCs was similar between TRPM2$^{-/-}$ and WT mice (Fig. 6*D*), the expression level of CD80, CD86, and CD83 molecules in that population was significantly lower in TRPM2$^{-/-}$ (Fig. 6*E*). These data suggest that TRPM2 plays a role in the differentiation and maturation of DCs, *in vitro* as well as *in vivo*.

TRPM2 controls DC migration and homing to lymph nodes on inflammation

Previous work has shown that TRPM2$^{-/-}$ mice exhibit impaired PMN infiltration during experimentally induced colitis (21). Therefore, we investigated whether TRPM2-mediated Ca^{2+} release may also play a role in DC chemotaxis and trafficking on chemokine or inflammatory stimuli. We isolated BMDCs from WT and TRPM2$^{-/-}$ mice and initially performed standard transwell chemotaxis assays using CXCL12 and CCL19 chemokines as stimuli. First, we examined whether TRPM2 deficiency affected chemokine-induced random migration in a chemotaxis assay by checkerboard analysis (25). We did not observe differences between immature WT and TRPM2$^{-/-}$ DCs in random migration toward CXCL12, as BMDCs were placed on the top chamber and the chemoattractant on both sides of the transwell membrane (**Fig. 7*A***). Next, we analyzed chemokine-induced directional migration by placing the chemokine only on the bottom chamber of the transwell (26). Figure 7*B* shows that both immature and mature TRPM2$^{-/-}$ BMDCs exhibited a significantly reduced chemotactic response to CXCL12 and CCL19, respectively.

To rule out the possibility that genetic TRPM2 depletion could result in disruption of additional signaling pathways that might affect DC chemotaxis, we performed TRPM2 protein depletion by siRNA methodology. We depleted TRPM2 channels by treating WT CD11c^{+} BMDCs with a specific TRPM2 siRNA. At 48 h after transfection of siRNA, TRPM2 transcripts or proteins were undetectable by standard RT-PCR and immunofluorescence (Fig. 7*C*). CD11c^{+} BMDCs treated with scrambled siRNA showed ability to migrate directionally in response to CXCL12 and CCL19, whereas TRPM2-siRNA-treated WT CD11c^{+} cells failed to migrate toward CXCL12 or CCL19, respectively (Fig. 7*D*). We confirmed that TRPM2 knockdown did not affect the plasma membrane expression of chemokine receptors in immature BMDCs, since flow cytometry revealed

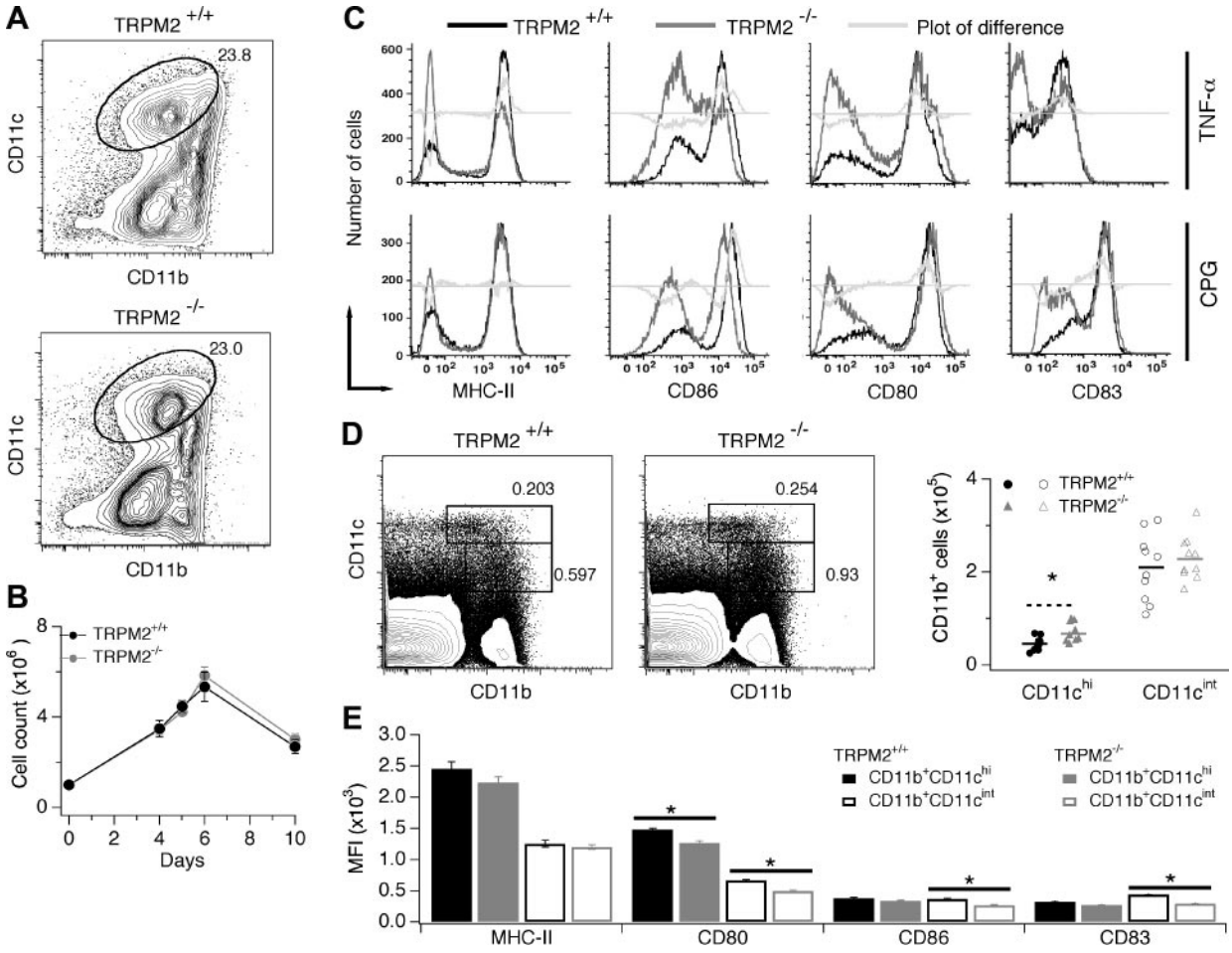

Figure 6. TRPM2-deficiency affects DC maturation. *A*) BMDCs were generated *in vitro* from WT and TRPM2$^{-/-}$ mice. Representative dot blot graphs indicating the percentage of DCs at d 6 of culture are shown. Samples were stained with APC-CD11c and eFluor 605-CD11b antibodies. *B*) Time course of DC proliferation of WT and TRPM2$^{-/-}$ BM cultures. *C*) BMDCs were matured by addition of TNF-α or CpG DNA, and the expression of maturation molecules class-II, CD86, CD80, and CD83 was analyzed by FACS. Changes in the maturation markers were assessed by comparison of TRPM2$^{+/+}$ BMDC histograms (black line) and TRPM2$^{-/-}$ BMDC (red line) and histogram differences (green line). Statistical significance of the differences was calculated by applying the $\chi(T)$ or PB test, wherein a value $T(X) > 4$ implies that the two distributions are different, with $P < 0.01$ (99% confidence). $T(X)$ values for TNF-α-treated DCs: class-II, 565; CD80, 990; CD86, 412; and CD83, 379. $T(X)$ values for CPG-treated DCs: class-II, 68; CD80, 1072; CD86, 499; and CD83, 495. Data are from 3 independent experiments (n=3). *D*) Splenic cell suspensions were prepared from WT and TRPM2$^{-/-}$ mice, and samples were stained as in *A*. Representative dot blot graphs indicating the percentage of CD11b^{+}CD11c^{hi} and CD11b^{+}CD11c^{int} DC populations and their total number. *E*) Splenic samples were stained as in *C*. Histograms represent mean fluorescence intensity (MFI) of MHC II, CD80, CD86, and CD83 in CD11b^{+}CD11c^{hi} (solid bars) and CD11b^{+}CD11c^{int} (open bars) DCs; $n = 10$. Paired Student's t test was applied for significance analysis; $P < 0.05$ was considered statistically significant.

similar levels of CXCR4, CCR5, and CCR7 in WT and TRPM2-knockout cells (Supplemental Fig. S4*A*). However, TRPM2-deficient DCs did not up-regulate the chemokine receptors CCR5, CXCR4, and CCR7 on TNF-α stimulation (Supplemental Fig. S4*A*). Because TRPM2$^{-/-}$ BMDCs showed impaired chemotaxis *in vitro*, we reasoned that the maturation and antigen-induced trafficking of immature DCs from the periphery to the secondary lymphoid organs could be also affected in the TRPM2$^{-/-}$ mice. To test this hypothesis, immature BMDCs (2×10^6/50 μl) from EGFP-TRPM2$^{-/-}$ mice or control mice (EGFP-C57BL/6) were injected into the right footpad of C57BL/6 mice 2 h before injection of *E. coli* (1×10^6 bacteria/footpad) to induce maturation and migration (33). Migratory DCs into the draining lymph nodes and nondraining lymph nodes were then analyzed by flow cytometry. Similarly to the *in vitro* experiments, the migration of EGFP-TRPM2$^{-/-}$ BMDCs to the lymph node was significantly impaired at 18 h after subcutaneous injection (Fig. 7*E*).

IP$_3$ receptors and lysosomal TRPM2 regulate Ca^{2+} signaling and chemotaxis in DCs

While defective Ca^{2+} responses to chemokines were apparent in individual cells of the TRPM2$^{-/-}$ BMDC populations, the average $[Ca^{2+}]_i$ in response to CXCL12 was also found to be significantly reduced in

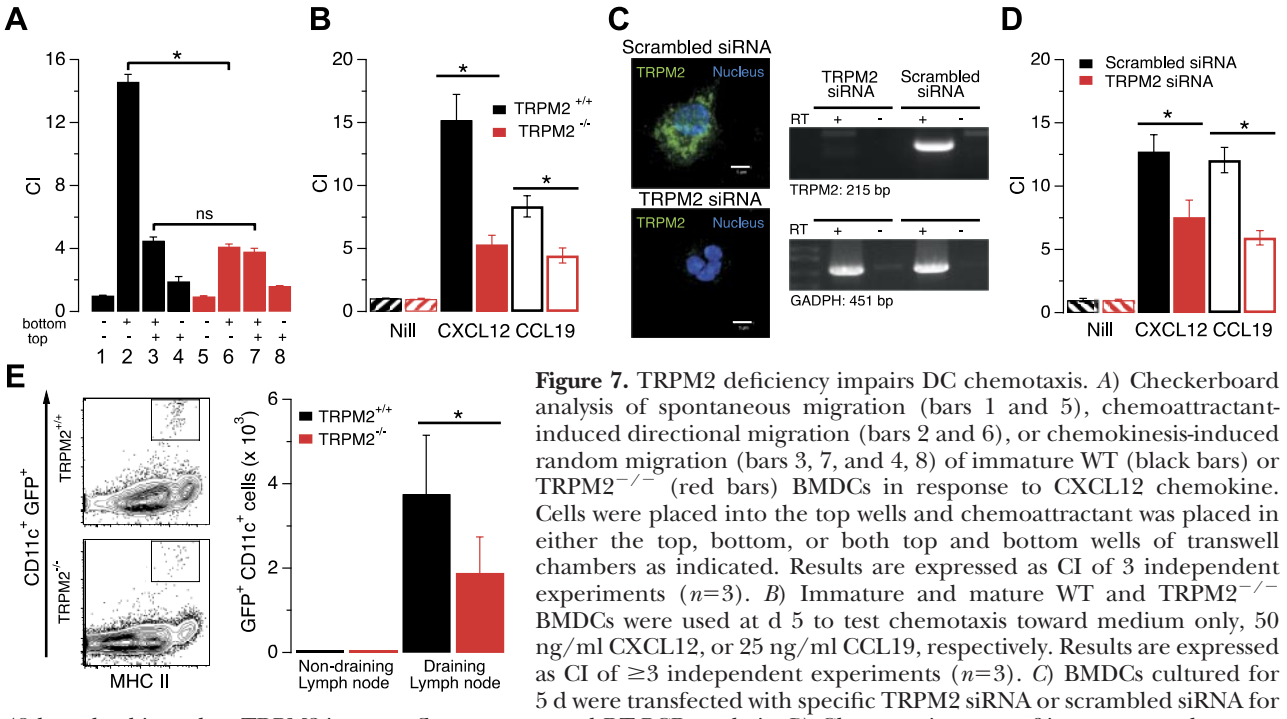

Figure 7. TRPM2 deficiency impairs DC chemotaxis. *A*) Checkerboard analysis of spontaneous migration (bars 1 and 5), chemoattractant-induced directional migration (bars 2 and 6), or chemokinesis-induced random migration (bars 3, 7, and 4, 8) of immature WT (black bars) or TRPM2$^{-/-}$ (red bars) BMDCs in response to CXCL12 chemokine. Cells were placed into the top wells and chemoattractant was placed in either the top, bottom, or both top and bottom wells of transwell chambers as indicated. Results are expressed as CI of 3 independent experiments (n=3). *B*) Immature and mature WT and TRPM2$^{-/-}$ BMDCs were used at d 5 to test chemotaxis toward medium only, 50 ng/ml CXCL12, or 25 ng/ml CCL19, respectively. Results are expressed as CI of ≥3 independent experiments (n=3). *C*) BMDCs cultured for 5 d were transfected with specific TRPM2 siRNA or scrambled siRNA for 48 h and subjected to TRPM2-immunofluorescence and RT-PCR analysis. *D*) Chemotaxis assays of immature and mature BMDCs treated with TRPM2 siRNA and scrambled siRNA. Chemotaxis was performed as in *A*. Results are expressed as CI of 3 independent experiments (n=3). *E*) Immature BMDCs (2×10^6/50 μl) from EGFP-*trpm2*$^{-/-}$ mice or EGFP-C57BL/6 were injected in the right footpad of 5 C57BL/6 mice 2 h before injection of *E. coli* (1×10^6 bacteria/footpad). To detect migratory BMDCs, single-cell suspensions from the right side popliteal and inguinal draining lymph nodes and nondraining lymph nodes (left side controls) were incubated with fluorescent anti-CD11c, anti-MHC class-II, and CD11b and analyzed by flow cytometry. Representative dot blot graphs indicate percentage of CD11c$^+$-GFP MHC$^+$ *trpm2*$^{+/+}$ DCs and *trpm2*$^{-/-}$ DCs and total number of migrated cells. Histograms represent total number of migrated BMDCs from 10 mice analyzed in 2 independent experiments. Values are means ± SE. *$P < 0.05$; Student's t test.

large TRPM2$^{-/-}$ BMDC populations in the absence of external Ca^{2+} or when WT BMDCs were treated with bafilomycin A (**Fig. 8*A***) in 1 mM external Ca^{2+}. These results are depicted as the mean fluorescence intensity of Fluo-3 on chemokine stimulation (Fig. 8). Treatment of WT DCs with bafilomycin A or concanamycin A (37, 38) significantly reduced CXCL12-induced chemotaxis (Fig. 8*B*), suggesting that lysosomal TRPM2-mediated Ca^{2+} release is important for DC chemotaxis.

Although the absence of TRPM2 clearly affected the Ca^{2+} responses of DCs, TRPM2$^{-/-}$ BMDCs can mobilize a sizeable amount of $[Ca^{2+}]_i$, likely through IP_3-mediated signaling downstream of chemokine receptors (39). To confirm that IP_3 also induces Ca^{2+}-release from DC intracellular stores (39, 40), we permeabilized WT BMDCs using a 4 μM digitonin-containing external solution and coapplied 100 μM IP_3. Supplemental Fig. S3*E* shows that IP_3 indeed evokes Ca^{2+} release in DCs. To determine the relative contribution of TRPM2 and IP_3R, we analyzed Ca^{2+} increases in WT and TRPM2$^{-/-}$ BMDCs. Ablation of TRPM2 reduced the CXCL12-induced Ca^{2+} transient by ~50% (Fig. 8*C*). $[Ca^{2+}]_i$ was suppressed further in TRPM2$^{-/-}$ BMDCs by 10 μM of the IP_3R inhibitor xestospongin C (XeC; refs. 41, 42). Additional XeC treatment of TRPM2$^{-/-}$ BMDCs suppressed CXCL12-induced chemotaxis (Fig. 8*D*) completely, indicating that both IP_3R and TRPM2 participate in chemokine-induced Ca^{2+} signaling and migration of DCs.

DISCUSSION

Migration of DCs from site of infections to lymphoid organs is central for the immune response. DC directional movement (chemotaxis) is initiated on activation of chemokine receptors in the plasma membrane and is regulated by the cytosolic Ca^{2+}-concentration ($[Ca^{2+}]_i$) (39–42). However, little is known about the proteins, including calcium channels that regulate Ca^{2+} signals during DC chemotaxis. We here demonstrate the functional expression of the ADPR-activated Ca^{2+}-permeable channel TRPM2 in mouse BMDCs. Our data show that TRPM2 expresses preferentially in lysosomes of immature and mature BMDCs but not in the plasma membrane, as confirmed by imunofluorescence, patch-clamp, and Ca^{2+} imaging experiments. In addition, our findings show that TRPM2 proteins are not accumulated within the cellular trafficking system, since TRPM2 staining is not observed in ER, Golgi, or mitochondria. Instead, TRPM2 staining overlaps with that of LAMP1 in immature DCs or DC-LAMP in mature DCs and may play a role in MHC class-II processing and antigen presentation by DCs.

Our studies demonstrate that TRPM2 represents a

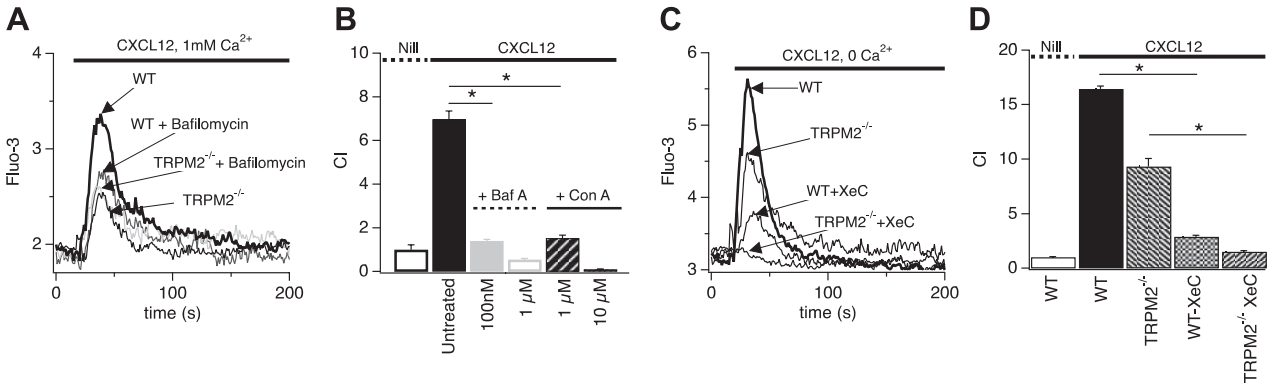

Figure 8. Both TRPM2 and IP_3R are required for normal Ca^{2+} release and chemotaxis in DCs. *A*) Ca^{2+} measurements in immature WT and TRPM2$^{-/-}$ BMDCs. Cells were loaded with Fluo-3 and then suspended in Hank's buffer without Ca^{2+}/Mg^{2+}. Cells were preincubated for 15 min in the presence or absence of 10 ng/ml bafilomycin A1, and then stimulated with CXCL12 (50 ng/ml). Accumulation of free Ca^{2+} was measured by FACS over the next 5 min. Arrows indicate intracellular Ca^{2+} responses of WT, WT + bafilomycin A1, TRPM2$^{-/-}$, and TRPM2$^{-/-}$ + bafilomycin A1. *B*) WT or TRPM2$^{-/-}$ immature BMDCs pretreated with bafilomycin A1 (Baf, 100 nM and 1 μM) or concanamycin A (Con A, 1 and 10 μM) or controls were placed in the top chamber of a transwell containing 50 ng/ml CXCL12 and 1.2 mM external Ca^{2+}. Cells that migrated to the bottom chamber in response to the chemotactic gradient were collected and enumerated by FACS. Values represent mean ± SE CI of triplicate cultures. *C*) Ca^{2+} measurements in DCs isolated from WT or TRPM2$^{-/-}$ mice preincubated for 15 min in the presence or absence of the IP_3 inhibitor XeC (10 μM), and then stimulated with CXCL12 (50 ng/ml). Free Ca^{2+} was measured by FACS over the next 5 min. Arrows indicate intracellular Ca^{2+} responses of WT, TRPM2$^{-/-}$, and TRPM2$^{-/-}$ cells + XeC. *D*) Chemotaxis assay as described in *B*. Cells were pretreated as in *C*. Values represent mean ± SE CI of triplicate cultures. Data are representative of 3 independent experiments (n=3). ANOVA was applied for significance analysis of CI (*B, D*) or area under curve (AUC) for the first 80 s (*A, C*). *$P < 0.05$.

functional ADPR-sensitive Ca^{2+} release channel in DCs (Fig. 2). Lysosomal Ca^{2+} release has not been documented previously in DCs, although lysosomes can function as Ca^{2+} stores (43). The treatment of DCs with antibiotics of the bafilomycin type, which prevents the acidification of lysosomes and endosomes and consequently empties lysosomal Ca^{2+} stores without affecting ER Ca^{2+} levels (37, 38), inhibited TRPM2-dependent Ca^{2+} release and Ca^{2+}-dependent chemotaxis in these cells. These findings were surprising, since earlier studies using a pharmacological competitor of ADPR, 8Br-ADPR, inhibited Ca^{2+} mobilization in CXCL12-stimulated BMDCs (9) and suggested a TRPM2-mediated Ca^{2+} entry mechanism in DCs (10). In the light of the current findings, it now appears that chemokine-receptor Ca^{2+} signaling in DCs is likely mediated by Ca^{2+} release and possibly secondary Ca^{2+} entry through store-operated Ca^{2+} entry (SOCE).

Our findings add a novel facet to TRPM2 function, since DCs are the first cell type found to express TRPM2 preferentially in intracellular compartments, whereas TRPM2 expression in human and mouse PMNs is restricted to the plasma membrane. Rat pancreatic β cells express TRPM2 in both lysosomal organelles and the plasma membrane (19). Interestingly, although immunofluorescent imaging data indicate localization of TRPM2 both at the plasma membrane and in intracellular structures of monocytes, ADPR-initiated Ca^{2+} release has yet to be shown for this cell type. The intracellular functional expression of TRPM2 is not an exclusive property of this channel, as other members of the TRP family (*e.g.*, TRPP2, TRPV1, and TRPM4) have also been reported to support release of Ca^{2+} from intracellular stores (44–46). In addition, recent studies have unveiled a new family of NAADP-gated Ca^{2+} release channels that are localized in lysosomes when expressed in HEK293 cells (47).

Optimal DC maturation *in vitro* and *in vivo* was reliant on TRPM2-dependent Ca^{2+} signaling, as demonstrated by reduced surface expression levels of costimulatory molecules CD80, CD86, MHC class-II, and CD83 (Fig. 4). A suboptimal mature population of DCs, $CD11b^{+}CD11c^{int}$, was also found in the spleen of TRPM2$^{-/-}$ mice, and this phenotype might predict additional DC-related functional defects in these mice, as DC maturation is critical for effective generation of immune responses. The molecular mechanism by which TRPM2 controls DC maturation remains unclear, although our results point to a regulatory role of Ca^{2+} signaling, in agreement with previous studies that showed a requirement for Ca^{2+} during DC maturation (6, 7, 48).

Chemotaxis of leukocytes is known to operate *via* chemokine receptors in the plasma membrane. These are GPCRs that activate phospholipase C (PLC), which subsequently produces IP_3 and diacylglycerol (DAG). IP_3 releases Ca^{2+} from the ER, leading to store depletion and a rise in $[Ca^{2+}]_i$ (1, 4, 5). Our results show that responses to chemokine receptors CXCR4 and CCR7 are impaired in TRPM2$^{-/-}$ BMDCs, and this correlates with diminished intracellular Ca^{2+} release in these cells. Interestingly, while siRNA treatment or genetic deletion of TRPM2 leads to a comparable suppression of chemotaxis in both mature and immature BMDCs *in vitro*, and defective migration of mature DCs *in vivo*, the

underlying intracellular Ca^{2+} signaling events exhibit some complexity. Immature TRPM2$^{-/-}$ BMDCs display strongly suppressed initial oscillatory activity and slightly suppressed secondary Ca^{2+} plateaus in the presence of external Ca^{2+}. Mature BMDCs, however, react faster to chemokine stimulation but then taper off in their Ca^{2+} response compared to WT. Removal of external Ca^{2+} reveals that only cells responding with one individual Ca^{2+}-release transient display suppressed Ca^{2+} release in immature TRPM2$^{-/-}$ BMDCs, while cells with Ca^{2+} oscillations are unaffected. In contrast, mature TRPM2$^{-/-}$ BMDCs show no difference in the Ca^{2+}-spike responders but produce fewer and reduced oscillatory events subsequent to the initial transient. These differential Ca^{2+} responses may reflect the change in chemokine receptor expression DCs undergo during the maturation process. Furthermore, the additional use of the IP_3R inhibitor XeC (43) reveals that suppression of both TPRM2 and IP_3R-mediated Ca^{2+} release abolishes chemokine-induced rises in $[Ca^{2+}]_i$ and chemotaxis. This finding indicates that TRPM2 and IP_3R are both critical for Ca^{2+} release in mouse DCs.

A recent study demonstrated impaired chemotaxis of SYT7-deficient neutrophils and splenocytes, a Ca^{2+}-dependent regulator of lysosomal fusion (49). It also showed that the small GTPases Rab27a and Rab3a, proteins known to regulate lysosome exocytosis, play a role in chemotaxis. These findings identify a molecular pathway required for chemotaxis that links chemoattractant-induced Ca^{2+} signals to lysosomal-dependent exocytosis and uropod release, in good agreement with our observations that Ca^{2+}-dependent lysosomal function is essential for cell migration of DCs.

Since Ca^{2+} release-activated Ca^{2+} channels (CRACs) are present in mouse DCs (34, 50), it is likely that SOCE plays a significant role in the chemoattractant-Ca^{2+} entry response of DCs. Indeed, we detected TRPM2-independent Ca^{2+} entry in TRPM2$^{-/-}$ DCs in the presence of external Ca^{2+} that followed the initial Ca^{2+} release transient, which could be explained by the activation of CRAC channels. One of the most intriguing observations of the present report was that TRPM2, although absent from the plasma membrane of DCs, still affected Ca^{2+} entry. Knockdown of TRPM2 actually accelerated the kinetics of Ca^{2+} entry, suggesting that TRPM2-mediated Ca^{2+} release can delay the activation of Ca^{2+} entry. Possible explanations for this phenomenon could be that lysosomal Ca^{2+} release occurring concomitantly with IP_3-induced release of Ca^{2+} from the ER causes Ca^{2+}-dependent inactivation of Ca^{2+} channels, and/or the lysosomal Ca^{2+} release is taken up by the ER, resulting in delayed activation of SOCE. Finally, another TRP channel from the melastatin family member, TRPM4, may further affect Ca^{2+} entry in DCs through regulation of the driving force for Ca^{2+} entry (33). In summary, our findings demonstrate a novel role of TRPM2 in the regulation of Ca^{2+} signaling of DCs, and suggest that inhibitors of TRPM2 function could potentially be used to block undesired DC-mediated responses. FJ

The authors thank S. Johne for technical support. This work was supported by the Research Institute at Nationwide Children's Hospital (S.P.-S. and A.S.-T.), U.S. National Institutes of Health grants GM063954 (R.P.) and GM078195 (A.F.), U.S. National Institute of Allergy and Infectious Diseases grant R01AI092117 (S.P.-S), and The Queen Emma Research Foundation (A.S.-T.). The John A. Burns School of Medicine (JABSOM) Histology and Imaging Core facility is supported by both Research Centers in Minority Institutions and Centers of Biomedical Research Excellence grants (G12-RR003061 and P20-RR016453). The JABSOM Molecular and Cellular Immunology Core facility is supported by COBRE grant 2P20RR018727-06. The funders had no role in study design, data collection and analysis, decision to publish, or preparation of the manuscript. The authors declare no conflicting financial interests.

REFERENCES

1. Choi, E. Y., Santoso, S., and Chavakis, T. (2009) Mechanisms of neutrophil transendothelial migration. *Front. Biosci.* **14,** 1596–1605
2. Kennedy, A. D., and DeLeo, F. R. (2009) Neutrophil apoptosis and the resolution of infection. *Immunol. Res.* **43,** 25–61
3. Steinman, R. M., and Banchereau, J. (2007) Taking dendritic cells into medicine. *Nature* **449,** 419–426
4. Randolph, G. J., Ochando, J., and Partida-Sanchez, S. (2008) Migration of dendritic cell subsets and their precursors. *Annu. Rev. Immunol.* **26,** 293–316
5. Selvatici, R., Falzarano, S., Mollica, A., and Spisani, S. (2006) Signal transduction pathways triggered by selective formylpeptide analogues in human neutrophils. *Eur. J. Pharmacol.* **534,** 1–11
6. Czerniecki, B. J., Carter, C., Rivoltini, L., Koski, G. K., Kim, H. I., Weng, D. E., Roros, J. G., Hijazi, Y. M., Xu, S., Rosenberg, S. A., and Cohen, P. A. (1997) Calcium ionophore-treated peripheral blood monocytes and dendritic cells rapidly display characteristics of activated dendritic cells. *J. Immunol.* **159,** 3823–3837
7. Koski, G. K., Schwartz, G. N., Weng, D. E., Gress, R. E., Engels, F. H., Tsokos, M., Czerniecki, B. J., and Cohen, P. A. (1999) Calcium ionophore-treated myeloid cells acquire many dendritic cell characteristics independent of prior differentiation state, transformation status, or sensitivity to biologic agents. *Blood* **94,** 1359–1371
8. Rubartelli, A., Poggi, A., and Zocchi, M. R. (1997) The selective engulfment of apoptotic bodies by dendritic cells is mediated by the alpha(v)beta3 integrin and requires intracellular and extracellular calcium. *Eur. J. Immunol.* **27,** 1893–1900
9. Partida-Sanchez, S., Gasser, A., Fliegert, R., Siebrands, C. C., Dammermann, W., Shi, G., Mousseau, B. J., Sumoza-Toledo, A., Bhagat, H., Walseth, T. F., Guse, A. H., and Lund, F. E. (2007) Chemotaxis of mouse bone marrow neutrophils and dendritic cells is controlled by adp-ribose, the major product generated by the CD38 enzyme reaction. *J. Immunol.* **179,** 7827–7839
10. Perraud, A. L., Fleig, A., Dunn, C. A., Bagley, L. A., Launay, P., Schmitz, C., Stokes, A. J., Zhu, Q., Bessman, M. J., Penner, R., Kinet, J. P., and Scharenberg, A. M. (2001) ADP-ribose gating of the calcium-permeable LTRPC2 channel revealed by Nudix motif homology. *Nature* **411,** 595–599
11. Sano, Y., Inamura, K., Miyake, A., Mochizuki, S., Yokoi, H., Matsushime, H., and Furuichi, K. (2001) Immunocyte Ca2+ influx system mediated by LTRPC2. *Science* **293,** 1327–1330
12. Csanady, L., and Torocsik, B. (2009) Four Ca2+ ions activate TRPM2 channels by binding in deep crevices near the pore but intracellularly of the gate. *J. Gen. Physiol.* **133,** 189–203
13. Kolisek, M., Beck, A., Fleig, A., and Penner, R. (2005) Cyclic ADP-ribose and hydrogen peroxide synergize with ADP-ribose in the activation of TRPM2 channels. *Mol. Cell* **18,** 61–69
14. Wehage, E., Eisfeld, J., Heiner, I., Jungling, E., Zitt, C., and Luckhoff, A. (2002) Activation of the cation channel long

transient receptor potential channel 2 (LTRPC2) by hydrogen peroxide. A splice variant reveals a mode of activation independent of ADP-ribose. *J. Biol. Chem.* **277,** 23150–23156
15. McHugh, D., Flemming, R., Xu, S. Z., Perraud, A. L., and Beech, D. J. (2003) Critical intracellular Ca2+ dependence of transient receptor potential melastatin 2 (TRPM2) cation channel activation. *J. Biol. Chem.* **278,** 11002–11006
16. Du, J., Xie, J., and Yue, L. (2009) Intracellular calcium activates TRPM2 and its alternative spliced isoforms. *Proc. Natl. Acad. Sci. U. S. A.* **106,** 7239–7244
17. Starkus, J. G., Fleig, A., and Penner, R. (2010) The calcium-permeable non-selective cation channel TRPM2 is modulated by cellular acidification. *J. Physiol.* **588,** 1227–1240
18. Yang, W., Zou, J., Xia, R., Vaal, M. L., Seymour, V. A., Luo, J., Beech, D. J., and Jiang, L. H. (2010) State-dependent inhibition of TRPM2 channel by acidic pH. *J. Biol. Chem.* **285,** 30411–30418
19. Lange, I., Yamamoto, S., Partida-Sanchez, S., Mori, Y., Fleig, A., and Penner, R. (2009) TRPM2 functions as a lysosomal Ca2+-release channel in beta cells. *Sci. Signal* **2,** ra23
20. Heiner, I., Eisfeld, J., and Luckhoff, A. (2003) Role and regulation of TRP channels in neutrophil granulocytes. *Cell Calcium* **33,** 533–540
21. Yamamoto, S., Shimizu, S., Kiyonaka, S., Takahashi, N., Wajima, T., Hara, Y., Negoro, T., Hiroi, T., Kiuchi, Y., Okada, T., Kaneko, S., Lange, I., Fleig, A., Penner, R., Nishi, M., Takeshima, H., and Mori, Y. (2008) TRPM2-mediated Ca2+influx induces chemokine production in monocytes that aggravates inflammatory neutrophil infiltration. *Nat. Med.* **14,** 738–747
22. Lange, I., Penner, R., Fleig, A., and Beck, A. (2008) Synergistic regulation of endogenous TRPM2 channels by adenine dinucleotides in primary human neutrophils. *Cell Calcium* **44,** 604–615
23. Beck, A., Kolisek, M., Bagley, L. A., Fleig, A., and Penner, R. (2006) Nicotinic acid adenine dinucleotide phosphate and cyclic ADP-ribose regulate TRPM2 channels in T lymphocytes. *FASEB J.* **20,** 962–964
24. Massullo, P., Sumoza-Toledo, A., Bhagat, H., and Partida-Sanchez, S. (2006) TRPM channels, calcium and redox sensors during innate immune responses. *Semin. Cell. Dev. Biol.* **17,** 654–666
25. Zigmond, S. H., and Hirsch, J. G. (1973) Leukocyte locomotion and chemotaxis. New methods for evaluation, and demonstration of a cell-derived chemotactic factor. *J. Exp. Med.* **137,** 387–410
26. Dunzendorfer, S., Kaser, A., Meierhofer, C., Tilg, H., and Wiedermann, C. J. (2000) Dendritic cell migration in different micropore filter assays. *Immunol. Lett.* **71,** 5–11
27. Fonfria, E., Murdock, P. R., Cusdin, F. S., Benham, C. D., Kelsell, R. E., and McNulty, S. (2006) Tissue distribution profiles of the human TRPM cation channel family. *J. Recept. Signal. Transduct. Res.* **26,** 159–178
28. Olah, M. E., Jackson, M. F., Li, H., Perez, Y., Sun, H. S., Kiyonaka, S., Mori, Y., Tymianski, M., and MacDonald, J. F. (2009) Ca2+-dependent induction of TRPM2 currents in hippocampal neurons. *J. Physiol.* **587,** 965–979
29. Heiner, I., Eisfeld, J., Warnstedt, M., Radukina, N., Jungling, E., and Luckhoff, A. (2006) Endogenous ADP-ribose enables calcium-regulated cation currents through TRPM2 channels in neutrophil granulocytes. *Biochem. J.* **398,** 225–232
30. Honing, S., Griffith, J., Geuze, H. J., and Hunziker, W. (1996) The tyrosine-based lysosomal targeting signal in lamp-1 mediates sorting into Golgi-derived clathrin-coated vesicles. *EMBO J.* **15,** 5230–5239
31. Bell, D., Chomarat, P., Broyles, D., Netto, G., Harb, G. M., Lebecque, S., Valladeau, J., Davoust, J., Palucka, K. A., and Banchereau, J. (1999) In breast carcinoma tissue, immature dendritic cells reside within the tumor, whereas mature dendritic cells are located in peritumoral areas. *J. Exp. Med.* **190,** 1417–1426
32. Bowman, E. J., Siebers, A., and Altendorf, K. (1988) Bafilomycins: a class of inhibitors of membrane ATPases from microorganisms, animal cells, and plant cells. *Proc. Natl. Acad. Sci. U. S. A.* **85,** 7972–7976
33. Barbet, G., Demion, M., Moura, I. C., Serafini, N., Leger, T., Vrtovsnik, F., Monteiro, R. C., Guinamard, R., Kinet, J. P., and Launay, P. (2008) The calcium-activated nonselective cation channel TRPM4 is essential for the migration but not the maturation of dendritic cells. *Nat. Immunol.* **9,** 1148–1156
34. Hsu, S., O'Connell, P. J., Klyachko, V. A., Badminton, M. N., Thomson, A. W., Jackson, M. B., Clapham, D. E., and Ahern, G. P. (2001) Fundamental Ca2+ signaling mechanisms in mouse dendritic cells: CRAC is the major Ca2+ entry pathway. *J. Immunol.* **166,** 6126–6133
35. Roederer, M., Moore, W., Treister, A., Hardy, R. R., and Herzenberg, L. A. (2001) Probability binning comparison: a metric for quantitating multivariate distribution differences. *Cytometry* **45,** 47–55
36. Rottembourg, D., Filippi, C. M., Bresson, D., Ehrhardt, K., Estes, E. A., Oldham, J. E., and von Herrath, M. G. (2010) Essential role for TLR9 in prime but not prime-boost plasmid DNA vaccination to activate dendritic cells and protect from lethal viral infection. *J. Immunol.* **184,** 7100–7107
37. Drose, S., Bindseil, K. U., Bowman, E. J., Siebers, A., Zeeck, A., and Altendorf, K. (1993) Inhibitory effect of modified bafilomycins and concanamycins on P- and V-type adenosinetriphosphatases. *Biochemistry* **32,** 3902–3906
38. Bai, L., Sagiv, Y., Liu, Y., Freigang, S., Yu, K. O., Teyton, L., Porcelli, S. A., Savage, P. B., and Bendelac, A. (2009) Lysosomal recycling terminates CD1d-mediated presentation of short and polyunsaturated variants of the NKT cell lipid antigen alphaGalCer. *Proc. Natl. Acad. Sci. U. S. A.* **106,** 10254–10259
39. Stolk, M., Leon-Ponte, M., Merrill, M., Ahern, G. P., and O'Connell, P. J. (2006) IP3Rs are sufficient for dendritic cell Ca2+ signaling in the absence of RyR1. *J. Leukoc. Biol.* **80,** 651–658
40. O'Connell, P. J., Klyachko, V. A., and Ahern, G. P. (2002) Identification of functional type 1 ryanodine receptors in mouse dendritic cells. *FEBS Lett.* **512,** 67–70
41. Gafni, J., Munsch, J. A., Lam, T. H., Catlin, M. C., Costa, L. G., Molinski, T. F., and Pessah, I. N. (1997) Xestospongins: potent membrane permeable blockers of the inositol 1,4,5-trisphosphate receptor. *Neuron* **19,** 723–733
42. Seale, A. P., Cooke, I. M., Hirano, T., and Grau, G. E. (2004) Evidence that IP3 and ryanodine-sensitive intra-cellular Ca2+ stores are not involved in acute hyposmotically-induced prolactin release in *Tilapia. Cell. Physiol. Biochem.* **14,** 155–166
43. Christensen, K. A., Myers, J. T., and Swanson, J. A. (2002) pH-dependent regulation of lysosomal calcium in macrophages. *J. Cell Sci.* **115,** 599–607
44. Qamar, S., Vadivelu, M., and Sandford, R. (2007) TRP channels and kidney disease: lessons from polycystic kidney disease. *Biochem. Soc. Trans.* **35,** 124–128
45. Turner, H., Fleig, A., Stokes, A., Kinet, J. P., and Penner, R. (2003) Discrimination of intracellular calcium store subcompartments using TRPV1 (transient receptor potential channel, vanilloid subfamily member 1) release channel activity. *Biochem. J.* **371,** 341–350
46. Cheng, H., Beck, A., Launay, P., Gross, S. A., Stokes, A. J., Kinet, J. P., Fleig, A., and Penner, R. (2007) TRPM4 controls insulin secretion in pancreatic beta-cells. *Cell Calcium* **41,** 51–61
47. Calcraft, P. J., Ruas, M., Pan, Z., Cheng, X., Arredouani, A., Hao, X., Tang, J., Rietdorf, K., Teboul, L., Chuang, K. T., Lin, P., Xiao, R., Wang, C., Zhu, Y., Lin, Y., Wyatt, C. N., Parrington, J., Ma, J., Evans, A. M., Galione, A., and Zhu, M. X. (2009) NAADP mobilizes calcium from acidic organelles through two-pore channels. *Nature* **459,** 596–600
48. Dauer, M., Obermaier, B., Herten, J., Haerle, C., Pohl, K., Rothenfusser, S., Schnurr, M., Endres, S., and Eigler, A. (2003) Mature dendritic cells derived from human monocytes within 48 hours: a novel strategy for dendritic cell differentiation from blood precursors. *J. Immunol.* **170,** 4069–4076
49. Colvin, R. A., Means, T. K., Diefenbach, T. J., Moita, L. F., Friday, R. P., Sever, S., Campanella, G. S., Abrazinski, T., Manice, L. A., Moita, C., Andrews, N. W., Wu, D., Hacohen, N., and Luster, A. D. (2010) Synaptotagmin-mediated vesicle fusion regulates cell migration. *Nat. Immunol.* **11,** 495–502
50. Matzner, N., Zemtsova, I. M., Nguyen, T. X., Duszenko, M., Shumilina, E., and Lang, F. (2008) Ion channels modulating mouse dendritic cell functions. *J. Immunol.* **181,** 6803–6809

Received for publication December 28, 2010.
Accepted for publication July 1, 2011.